Accurate validation of experimental results of interdiffused InGaAs/GaAs strained quantum wells by suitable numerical methods (1)

Miguel Prol, Alfonso Moredo-Araújo, F. Javier Fraile-Peláez

Dept. de Tecnologías de las Comunicaciones, Universidad de Vigo, ETS Ingenieros de Telecomunicación. E-36200 Vigo, Spain

Rafael Gómez-Alcalá

Dept. de Informática, Universidad de Extremadura, Escuela Politécnica. E-10071 Cáceres, Spain

ABSTRACT

In this paper, we make use of the Galerkin method along with the Green´s function method to analyze structures of InGaAs/GaAs strained quantum wells. The optical absorption coefficient is calculated and the achieved agreement with published experimental data is significantly better than previously reported predictions, thus providing a stronger confirmation of the validity and accuracy of the theoretical model. In addition, the computational efficiency is remarkably improved with the developed procedure.

Key words: InGaAs/GaAs quantum well, interdiffusion, strain, Green´s function, Galerkin method.

(1) *Manuscript of the article published in* Superlattices and Microstructures, vol. 30, 61-67 (2001).

1. INTRODUCTION

The development of quantum well (QW) structures has strongly influenced the developement of a great variety of optoelectronic devices such as electroabsorption modulators, detectors, lasers, and waveguides. In this context, strained layer quantum wells play an important role because of their interesting properties arising as a result of lattice mismatch. A growing interest exists in the use of nonsquare quantum wells with a nonlinear graded bandgap profile, such as those produced by thermal interdiffusion of In and Ga in $In_xGa_{1-x}As/GaAs$ quantum wells. Interesting fundamental quantum-mechanical phenomena can be controlled experimentally by tailoring the band structure of the semiconductor heterojunction profiles. The interdiffusion process modifies the originally square quantum well into an error-function compositional profile, and this leads to important changes in the energy bandgap and the heavy hole (HH)-light hole (LH) energy splitting caused by the strain effects. These changes in the optical properties of interdiffused QWs produce an overall blue shift of the optical absorption edge that provides a wavelength tuning range useful for optoelectronic applications.

In a previous work [1], we presented a model to show the influence of the diffusion length and the As-grown Indium mole fraction and well width on the absorption characteristics of the quantum structures. The model takes into account both the continuum and bound states due to the Coulomb interaction between electrons and holes in the excitonic absorption spectrum. To model the polarization-dependent optical absorption in this type of heterostructure we used an exciton Green's function approach. Such a model is quite general and can be applied to some degree of approximation to a quantum well potential with an arbitrary profile. One limitation of the model is the parabolic band structure with no valence band-mixing accounted for. However,

the compressive strain in the pseudomorphic heterostructure and the corresponding separation between the heavy-hole and light-hole bands greatly reduces the band mixing effects.

The model can be summarized in a two-step sequence: (1) The allowed energy levels for each subband (and the corresponding associated wavefunctions) are calculated taking into account both disordering and strain effects, but not the exciton effects due to the coulombic attraction between electrons in the conduction band and holes in the valence band. In this stage, all the carrier effective masses are considered to be *x*-dependent, *i.e.*, *z*-dependent (see Figure 1). (2) The necessary corrections in the energy values due to the coulombic interaction are obtained through a momentum-space exciton equation.

(FIGURE 1)

Step 1 was implemented previously by the transference-matrix method (TMM). In general, TMM is a simple method, but not always accurate. Moreover, it breaks down when complex structures with many wells are analized.

In this paper we shall analyze a single quantum well yet we shall use the Galerkin method [2, 3] to calculate the first estimate of the energies and wavefunctions; as we shall see, this will result in a significant improvement over the TMM performance. For most of the different material parameters involved in the analysis we shall employ expressions and data from the literature [4-7]. For example, we considered an initial 70:30 conduction:valence band discontinuity ratio (Q_c : Q_v) [6]. The *x*-dependence for the unstrained band gap energy is [7]:

$$E_g(300K) = 1.433 - 1.554x + 0.475x^2 . \quad (1)$$

Other parameters, such as the excitonic linewidth and the relative dielectric constant for the $In_xGa_{1-x}As$ material, have been estimated by us. Hereafter it will be understood that, when no reference is provided for an expression or parameter value, it has been calculated by the authors [1, 8]. See also Table 1 for a summary of some of the parameters used.

(TABLE 1)

2. THEORY

Starting from an As-grown quantum well with a square potential, the disordering introduced by the interdiffusion process results in a graded compositional profile that is approximated by an error function [9],

$$x(z) = \frac{x_0}{2}\left[\operatorname{erf}\left(\frac{L_z + 2z}{4L_d} \right) + \operatorname{erf}\left(\frac{L_z - 2z}{4L_d} \right) \right], \tag{2}$$

where L_z is the As-grown width of the well, z is the growth direction and x_0 is the As-grown In mole fraction in the center of the well, $z = 0$ (see Figure 1).

The energy levels and the wavefunctions will first be calculated by the Galerkin method. Next, the excitonic correction will be computed through the following momentum-space exciton equation:

$$E_{nm}(\mathbf{k})\phi^X_{nm}(\mathbf{k}) - \sum_{n'm'}\sum_{\mathbf{k}'} \left\langle nm \left| V_{\mathbf{k}-\mathbf{k}'} \right| n'm' \right\rangle \phi^X_{n'm'}(\mathbf{k}') = E_X \phi^X_{nm}(\mathbf{k}). \tag{3}$$

Equation (3) is solved by a Green's function-based method [10]. Green's method permits to compute the absorption coefficient easily well beyond the first absorption peaks, to include C-HH2, C-LH2 and even further; we have verified this feature experimentally with square wells [8]

and, from our numerical simulations, we expect the method to have the same robustness for disordered wells as well. For the Green's method, a reduced effective mass is used:

$$1/m_r = 1/m_e + 1/m_h . \tag{4}$$

Asigning to each transversal effective mass its value at the center of the well (for the corresponding sub-band) would be very accurate for a square quantum-well with large barriers and wavefunctions strongly confined inside the well, where we can assume that the mass is constant. This not being the case, we have chosen to use constant averaged masses. This approach turns out to be a very reasonable simplification, as we shall see in the results. For example,

$$\bar{m}_x = \int m_x(z)\psi^2(z)dz \text{ , where } \int \psi^2(z)dz = 1 . \tag{5}$$

Next, the corresponding HH and LH longitudinal masses are given in terms of the Luttinger parameters:

$$m_{hhz} = \frac{1}{\gamma_1 - 2\gamma_2} \text{ , } m_{lhz} = \frac{1}{\gamma_1 + 2\gamma_2} \text{ , } m_{hh||} = \frac{1}{\gamma_1 + \gamma_2} \text{ , } m_{lh||} = \frac{1}{\gamma_1 - \gamma_2} . \tag{6}$$

The system we analyze is a 100 Å $In_{0.2}Ga_{0.8}As$ square well between two large GaAs barriers. The introduction of the interdiffusion effects results in a graded mismatch between the lattice parameters in the pseudomorphic heterostructure. Both the interdiffusion and the compressive strain modify the confinement profiles and the interband transitions. In Figure 1 the solid line shows, first, the changes applied to the 'initially unstrained' bandgap (the square profile) showing the effects of disordering (eq. (2)). Then we introduce the effects of strain and spin-orbit coupling. This is done in two steps also sketched in Figure 1 (note that, for better definition, the bandgap energy in this figure is not in scale with the depth of the confinement wells). We introduce the effect caused by the biaxial component of strain (hydrostatic strain) first:

$$\delta E_{hy} = -2a(x)(1-\frac{c_{12}}{c_{11}})\varepsilon(x)\,, \tag{7}$$

where $a(x)$ is the hydrostatic deformation potential, c_{11} and c_{12} are the stiffness constants, and $\varepsilon(x) = (a_0 - a_0(x))/a_0$ is the in-plane strain (negative for compressive strain). As is well-known, this increases the energy transition between the conduction and valence bands at the Brillouin zone center Γ (and reduces the relative depth of the well in each band). At this point, the confinement profile for the heavy-hole and light-hole band still coincide. Next, the effect of the uniaxial component of strain (uniaxial shear strain [4]) is considered:

$$\begin{gathered} Q_{\varepsilon} = -b(x)\left(1+\frac{2c_{12}}{c_{11}}\right)\varepsilon(x) \\ Q_{\varepsilon HH} = Q_{\varepsilon} \ \text{(HH band)} \ ; \ Q_{\varepsilon LH} = -\frac{1}{2}\left(Q_{\varepsilon} - \Delta + \sqrt{\Delta^2 + 9Q_{\varepsilon}^2 + 2\Delta Q_{\varepsilon}}\right) \ \text{(LH band)}. \end{gathered} \tag{8}$$

This splits the formerly common HH and LH confinement profiles (removing the degeneracy of the parabolic bands at Γ) while there is no further change in the conduction confinement profile. For the total conduction-valence bandedge transitions we have

$$E_{C-x} = E_C - E_x = E_g - \delta E_{hy} + Q_{\varepsilon x} \ \ (x = \text{HH, LH})\,. \tag{9}$$

3. RESULTS

Figure 2 shows the wavefunctions of the first two energy levels in the conduction band. The differences between using the TMM and the Galerkin method are negligible. A similar behavior is shown by the HH and LH wavefunctions. Table 2 lists the energy levels as computed by both methods, indicating the percentage of error.

(FIGURE 2)

(TABLE 2)

In Figure 3, the absorption spectra are plotted for several values of L_d. Such spectra have been calculated as explained in [10], with the wavefunctions and energies computed both by the TMM and Galerkin method. Figure 3 (a), corresponding to a square well with $L_d = 0$, shows a qualitative coincidence between the graphics of the absorption coefficient, but also remarkable quantitative diferences. Some of the ripple appearing in the curve if the TMM is used (due to a mathematical artifact) actually disappears when the more accurate Galerkin method is employed. Note for example the second peak, which appears higher and cleaner than if predicted through the TMM calculations. Similar diferences are found for the cases where $L_d = 20$ Å and $L_d = 40$ Å.

(FIGURE 3)

Another outstanding advantage of this new approach is related to the computation time of the overall simulation. In Figure 4 we show the total execution times for the calculation of the absorption coefficients where the main feature is the great improvement in the relative differences of times achieved with the Galerkin method. (The absolute timings, being computer-dependent, are not so relevant.)

(FIGURE 4)

4. CONCLUSIONS

The use of Galerkin's method has led to more accurate, reliable results, unveiling previous numerical defficiencies. Galerkin's method has better performance to accurate compute energy levels and wavefunctions of higher order than the TMM, which explains the differences observed in the absorption curves. This provides support to the theoretical methods developed from [9], as the major quantitative discrepancies between measurements and computations were due to the deficiencies of the numerical approach rather than to the physical models used. Very good agreement is achieved with other results previously reported in the literature [5, 11].

Moreover, the presented method has the added benefit of a significantly improved computational efficiency as compared with other methods.

ACKNOWLEDGMENTS

The authors wish to thank Prof. S. L. Chuang for his support and encouragement.

REFERENCES

[1] M. Prol, C. S. Chang, and S. L. Chuang, "Exciton Green´s function method for interdiffused InGaAs/GaAs strained quantum wells," in *Physics and Simulation of Optoelectronic Devices VII, Proceedings of SPIE*, edited by P. Blood, A. Ishibashi, and M. Osinski (San Jose, 1999), Vol. 3625, p. 495.

[2] R. Gómez-Alcalá, C. Mejuto-Vila, F. J. Fraile-Peláez and I. Esquivias, Superlatt. Microstruct. **17**, 277 (1995).

[3] C. A. J. Fletcher, *Computational Galerkin Methods* (Springer-Verlag, 1984).

[4] S. L. Chuang, *Physics of Optoelectronic Devices* (Wiley, 1995).

[5] J. Micallef, E. H. Li, and B. L. Weiss, Superlatt. Microstruct. **13**, 125 (1993).

[6] J. Bohrer, A. Krost, T. Wolf, and D. Bimberg, Phys. Rev. B **47**, 6439 (1993).

[7] S. Paul, J. B. Roy, P. K. Basu, J. Appl. Phys. **69**, 827 (1991).

[8] M. Prol, C. S. Chang, S. L. Chuang, and T. F.Young, "Estimation of Material Parameters in InGaAs/InAlAs MQW by an Exciton Green's Function-Based Model," in *Proceedings of ICECOM***,** edited by and J. Bartolic (Dubrovnik, 1997), p. 150.

[9] G. P. Kothiyal and P. Bhattacharya, J.Appl. Phys. **63**, 2760 (1988).

[10] S. L. Chuang, S. Schmitt-Rink, D. A. B. Miller, and D. S. Chemla, Phys. Rev. B **43**, 1500 (1991).

[11] J. Micallef, E. H. Li, and B. L. Weiss, Superlatt. Microstruct. **13**, 315 (1993).

TABLE CAPTIONS

Table 1. Material parameters for $In_xGa_{1-x}As$ material.

a_0 : lattice parameter

b : shear deformation potential

c_x : stiffness constants

dE_g/dP : hydrostatic pressure coefficient

Δ_0 : spin-orbit splitting

m_x : effective masses

Table 2. Energy levels (in eV) for the conduction, heavy-hole, and light-hole bands.

FIGURE CAPTIONS

Figure 1. Evolution of the confinement profile when introducing consecutively the effects of interdiffusion (solid line), biaxial strain (dotted line) and uniaxial strain (dash-dotted line). There is no change in the conduction confinement profile due to uniaxial strain (the bandgap energy in the figure is not in scale with the depth of the confinement wells).

Figure 2. Wavefunctions in the conduction band calculated with the TMM (dashed line) and Galerkin (solid line) methods.

Figure 3. Absorption spectra for different values of the diffusion length.

Figure 4. Comparison between the total execution times of the TMM and Galerkin methods.

TABLES

	$In_xGa_{1-x}As$
a_0	$5.6533 + 0.4051x$ [Å]
B	$-1.7-0.1\,x$ [eV]
c_{11}	$11.88 - 3.55\,x$ [$\times 10^{11}$ dyn/cm^2]
c_{12}	$5.38 - 0.854\,x$ [$\times 10^{11}$ dyn/cm^2]
dE_g/dP	$11.5 - 1.5\,x$ [$\times 10^{-6}$ eV/bar]
Δ_0	$0.341 - 0.09\,x + 0.14\,x^2$ [eV]
m_e	$0.067 - 0.044\,x$
m_{HH}	$0.34 - 0.077\,x$
m_{LH}	$0.094 - 0.067\,x$

Table 1

	TMM	Galerkin	Δ %
E_1^C	0.033824	0.032486	4.1207
E_2^C	0.092431	0.090646	1.9689
E_1^{HH}	0.014203	0.013328	6.5612
E_2^{HH}	0.041672	0.040627	2.5722
E_1^{LH}	0.010855	0.010196	6.4610
E_2^{LH}	0.015824	0.015379	2.8911

Table 2

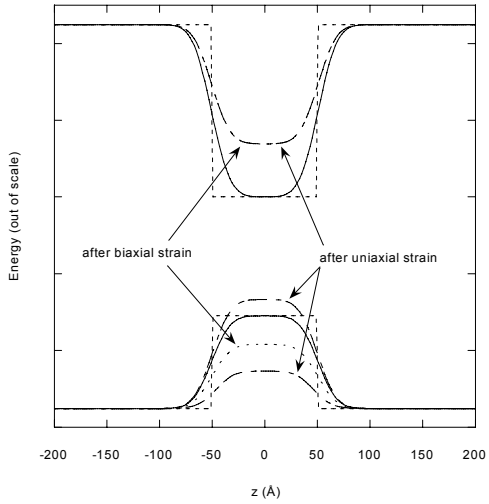
Energy (out of scale)
after biaxial strain
after uniaxial strain
-200
-150
-100
-50
0
50
100
150
200
z (Å)

Figure 1.

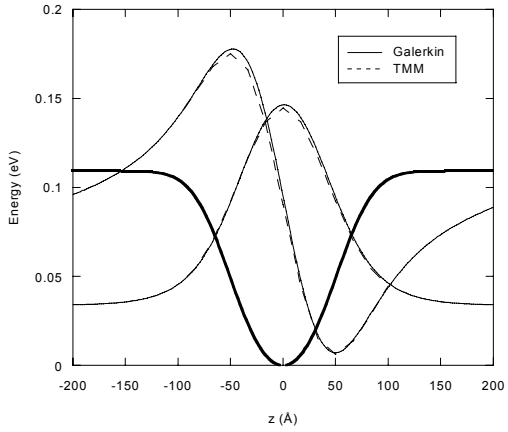
Galerkin
TMM
Energy (eV)
z (Å)
0.2
0.15
0.1
0.05
0
-200
-150
-100
-50
0
50
100
150
200

Figure 2.

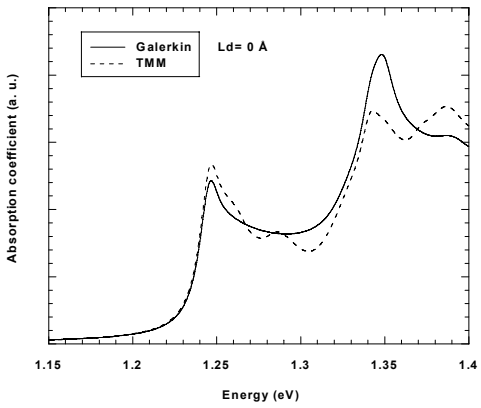
Galerkin
TMM
Ld= 0 Å
Absorption coefficient (a. u.)
1.15
1.2
1.25
1.3
1.35
1.4
Energy (eV)

(a)

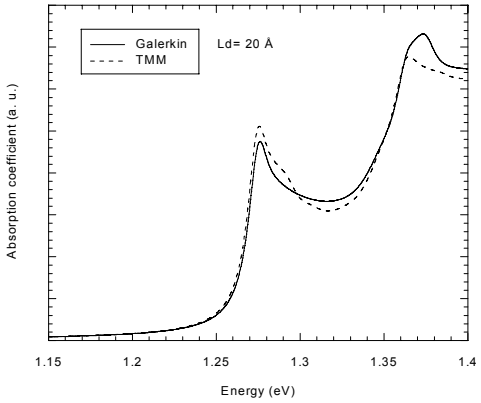
Galerkin
TMM
Ld= 20 Å
Absorption coefficient (a. u.)
1.15
1.2
1.25
1.3
1.35
1.4
Energy (eV)

(b)

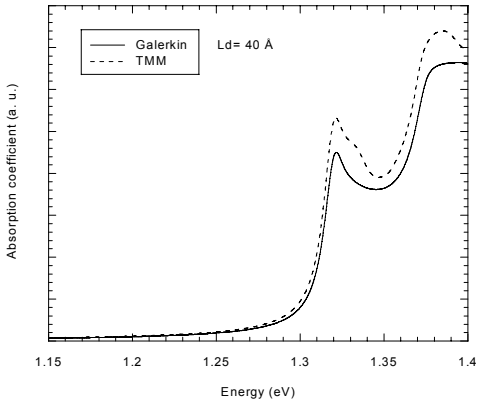
Galerkin
TMM
Ld= 40 Å
Absorption coefficient (a. u.)
1.15
1.2
1.25
1.3
1.35
1.4
Energy (eV)

(c)

Figure 3.

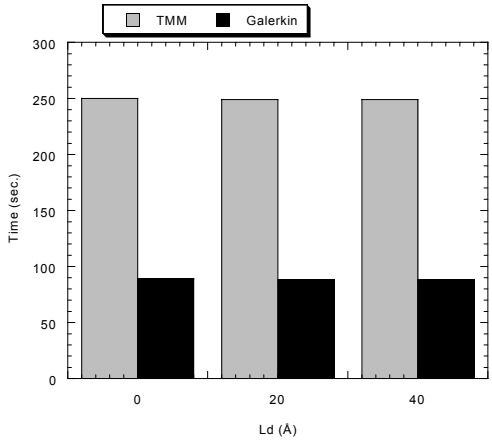

Figure 4.